

## NUMERICAL ANALYSIS OF MULTIPHASE SOLID-GAS FLOW WITH EULERIAN MODELS AND KINETIC THEORY CLOSURE

Cesar Venier<sup>a</sup>, Santiago Marquez Damian<sup>a</sup>, Damian Ramajo<sup>a</sup> and Norberto Nigro<sup>a</sup>

<sup>a</sup>*International Center for Computational Methods in Engineering (CIMEC)*  
INTEC-UNL-CONICET, Guemes 3450 S3000GLN Santa Fe, Argentina

**Keywords:** CFD, Multiphase Flow, Fluidized Bed, Drag Model, Kinetic Theory of Granular Flow

**Abstract.** Multiphase solid-gas flows may be found in many industrial applications, from oil refining processes to hydrogen production reactors. In particular, we focus our interest in the dynamics of solid particles in a circulating fluidized bed riser of a Fluid Catalytic Cracking (FCC) unit, in which the solid particles distribution is one of the main variables in the global efficiency of the unit. In the last decades, much effort has been put in the development of Euler-Euler models with granular energy coupling to simulate this kind of problems due to the good balance between computational cost and accuracy of the numerical solution. In this work, in order to have a closure with the Navier-Stokes equations for the solid phase, we use the kinetic theory of granular flow with solid pressure and stress tensor models, while Wen-Yu and Ergun correlations are used to calculate the drag coefficients. All the numerical simulations are carried out with the fully unstructured open source code OpenFOAM<sup>®</sup>, based on the finite volume method. In addition, an iterative procedure based on a combination of PISO and SIMPLE method (called PIMPLE) is adopted and a proper discussion of its benefits is performed. To validate the solver, we present two widely studied multiphase flow problems. The first one consists on a sedimentation column starting from a uniform solid volume fraction suspension. The second one is based on a falling block of solid particles in a pure gas environment. Finally, we study a problem of a fluidized bed of particles with a constant gas injection from below. For this case, we are able to verify the good performance of the solver. In order to do this, we analyze the time and space average profiles of the solid volume fraction in comparison with the numerical and experimental results from several authors.

## 1 INTRODUCTION

In the context of solid-gas multiphase flows, the Circulating Fluidized Bed (CFB) reactors are commonly used in many industrial applications such as agriculture, pharmaceutical, chemical and energy production processes due to the low pressure drops, uniform temperature distributions and high energy and mass-transfer rates. A riser of a Fluid Catalytic Cracking (FCC) unit uses this kind of configuration, in which the interaction between gas-solid and solid-solid particles directly affects in the global efficiency of the process. This leads to the need of a proper understanding of the natural phenomena involving fluidized bed multiphase systems (Min et al., 2010; Li et al., 2011) and FCC units in particular (Ramajo et al., 2010; Almuttahir and Taghipour, 2008).

The design of a commercial-scale CFB system is usually based on the previously obtained data of pilot-scale experiments, which are expensive, often difficult to setup and time consuming. Also, with the development of high performance computers and the advances in numerical techniques and algorithms, Computational Fluid Dynamics (CFD) becomes a strong tool to aid and complement the experimental approach for the design of such systems.

The Euler-Euler (EE) method and the Lagrange-Euler (LE) method are the two main approaches used to simulate gas-solids flows. While the LE method, in which the equations of motion are solved for each solid particle, gives high precision describing the solid-gas and solid-solid interactions, it requires a strong amount of computational resources to simulate the physics of real CFB problems. On the other hand, with the EE method, both phases are described as an interpenetrating continua, provides a good balance between the computational costs and accuracy in the description of the flow. In this present work, we opt for the EE approach with kinetic theory of granular flow which gives closure to the conservation equations (Gidaspow, 1994; Van Wachem, 2000).

Here we use a multiphase solver called *twoPhaseEulerPimpleFoam* (Passalacqua and Fox, 2011) developed and implemented into the open-source code OpenFOAM® (OpenCFD-OpenFOAM, 2010), to carry out the simulations. This solver is an improved version of the *twoPhaseEulerFoam*, in which the possibility to simulate an arbitrary number of dispersed phases and a conservative treatment of the phase momentum equations, were added. The solver also provides a great variety of drag models and kinetic theory models.

As a reminder of the present work, the next sections are organized as follows. In Section 2, we describe the equations involved in the model. The Section 3 briefly describes the numerical approach implemented in the solver. Finally, in Section 4 we present the results for two test cases and the results and analysis of a standard fluidized bed case.

## 2 MULTIPHASE MODEL

The Euler-Euler two phase model implemented in the open-source finite volume based program OpenFOAM® was used to carry out the simulations. This model is based in the fact that both phases are treated as interpenetrating continua (Gidaspow, 1994), the concept of phase volume fraction is introduced and the condition  $\sum_i \alpha_i = 1$  is verified. The continuity and momentum equations for the dispersed phase are:

$$\begin{aligned} \frac{\partial}{\partial t}(\alpha_s \rho_s) + \nabla \cdot (\alpha_s \rho_s \mathbf{u}_s) &= 0 \\ \frac{\partial}{\partial t}(\alpha_s \rho_s \mathbf{u}_s) + \nabla \cdot (\alpha_s \rho_s \mathbf{u}_s \mathbf{u}_s) &= \nabla \cdot (\alpha_s \boldsymbol{\tau}_s) - \alpha_s \nabla p - \nabla p_s + \alpha_s \rho_s \mathbf{g} + K_{sg}(\mathbf{u}_g - \mathbf{u}_s) \end{aligned} \quad (1)$$

On the other hand, the conservation equations for the continuous phase are:

$$\begin{aligned} \frac{\partial}{\partial t}(\alpha_g \rho_g) + \nabla \cdot (\alpha_g \rho_g \mathbf{u}_g) &= 0 \\ \frac{\partial}{\partial t}(\alpha_g \rho_g \mathbf{u}_g) + \nabla \cdot (\alpha_g \rho_g \mathbf{u}_g \mathbf{u}_g) &= \nabla \cdot (\alpha_g \boldsymbol{\tau}_g) - \alpha_g \nabla p + \alpha_g \rho_g \mathbf{g} + K_{sg}(\mathbf{u}_s - \mathbf{u}_g) \end{aligned} \quad (2)$$

Here, both phases are treated as Newtonian fluids and the stress tensors are defined as:

$$\begin{aligned} \boldsymbol{\tau}_g &= \mu_g [\nabla \mathbf{u}_g + \nabla \mathbf{u}_g^T] - \frac{2}{3} \mu_g (\nabla \cdot \mathbf{u}_g) \mathbf{I} \\ \boldsymbol{\tau}_s &= \mu_s [\nabla \mathbf{u}_s + \nabla \mathbf{u}_s^T] + (\lambda_s - \frac{2}{3} \mu_s) (\nabla \cdot \mathbf{u}_s) \mathbf{I} \end{aligned} \quad (3)$$

In order to solve the governing equations, several unknown terms require modeling. These models are known as closure laws.

If we are treating a dispersed phase with relatively small particles and large densities, the interphase drag force dominates over the other forces such as lift and virtual mass (Ranade, 2002). Therefore, the  $K_{sg}$  coefficient has just a drag contribution. A list of the available models are detailed in Table 1:

Author	Drag Model
Ergun	$K_{sg} = 150 \frac{\mu_g \alpha_s^2}{d_p^2 \alpha_g^2} + 1.75 \frac{\rho_g \alpha_s}{d_p \alpha_g}  \mathbf{u}_g - \mathbf{u}_s $
Wen-Yu	$K_{sg} = 0.75 \frac{C_d \alpha_s \alpha_g^{-1.65} \rho_g  \mathbf{u}_g - \mathbf{u}_s }{d_p}$
Gidaspow	$K_{sg} = \begin{cases} \text{Ergun Model} & , \alpha_s > 0.2 \\ \text{Wen-Yu Model} & , \alpha_s < 0.2 \end{cases}$
Schiller-Naumann	$K_{sg} = 0.75 \frac{C_d \alpha_s \alpha_g \rho_g  \mathbf{u}_g - \mathbf{u}_s }{d_p}$
Syamlal-O'Brien	$K_{sg} = 0.75 \frac{C_\epsilon \alpha_s \alpha_g \rho_g  \mathbf{u}_g - \mathbf{u}_s }{d_p v_{ts}^2}$
Gibilaro	$K_{sg} = 17.3 \frac{\mu_g}{d_p^2 \alpha_g^{2.8}} + 0.336 \frac{\rho_g}{d_p \alpha_g^{2.8}}  \mathbf{u}_g - \mathbf{u}_s $

Table 1: Drag models

Fluidized systems are an example of multiphase flow in which the gravity and drag are the dominant forces. But when the density of particles is greater, the frictional stresses becomes preponderant. Therefore, for general cases, it is recommended to use a model that takes into account both scenarios, such as Gidaspow and Syamlal-O'Brien drag models.

The coefficients  $C_d$ ,  $C_e$ ,  $v_{rs}$  and  $Re_p$  are defined as:

$$C_d = \begin{cases} \frac{24}{Re_p}(1 + 0.15Re_p^{0.687}), & Re_p < 1000 \\ 0.44, & Re_p \geq 1000 \end{cases}, \quad C_e = \left[0.63 + \frac{4.8}{(Re_p/v_{rs})^{0.5}}\right]^2 \quad (4)$$

$$v_{rs} = 0.5 \left( A - 0.06Re_p + \sqrt{(0.06Re_p)^2 + 0.12Re_p(2B - A) + A^2} \right) \quad (5)$$

$$A = \alpha_g^{4.14}, \quad B = \begin{cases} 0.8\alpha_g^{1.28}, & \alpha_g \leq 0.85 \\ \alpha_g^{2.65}, & \alpha_g > 0.85 \end{cases} \quad (6)$$

$$Re_p = \frac{\rho_g d_p |\mathbf{u}_g - \mathbf{u}_s|}{\mu_g} \quad (7)$$

The kinetic theory of granular flow (Gidaspow, 1994; Van Wachem, 2000) introduces the concept of granular temperature ( $\theta_s$ ) to have closure with the conservation equations. Therefore, the properties of the dispersed phase are function of this granular temperature, which is determined by solving the granular energy transport equation:

$$\frac{3}{2} \left[ \frac{\partial}{\partial t} (\alpha_s \rho_s \theta_s) + \nabla \cdot (\alpha_s \rho_s \mathbf{u}_s \theta_s) \right] = (-p_s \mathbf{I} + \boldsymbol{\tau}_s) : \nabla \mathbf{u}_s + \nabla \cdot (\kappa_s \nabla \theta_s) - \gamma_s + J_{vis} \quad (8)$$

The solid stress tensor contains shear and bulk viscosities arising from particle momentum exchange due to translation and collision. A frictional component of the viscosity can also be included to account the effect of the viscous-plastic transition when the maximum solids volume fraction is reached.

$$\mu_i = \mu_{i,col} + \mu_{i,kin} + \mu_{i,fric} \quad (9)$$

Schaeffer (1987) proposed the following models to calculate these parameters:

$$\mu_{s,col} = \frac{4}{5} \rho_s \alpha_s^2 d_p g_0 (1 - e_p) \left( \frac{\theta_s}{\pi} \right)^{1/2} \quad (10)$$

$$\mu_{s,fric} = 0.5 p_s I_{2D}^{-1/2} \sin(\phi)$$

The particle bulk viscosity is given by:

$$\lambda_s = \frac{4}{3} \rho_s \alpha_s^2 d_p g_0 (1 - e_p) \left( \frac{\theta_s}{\pi} \right)^{1/2} \quad (11)$$

And the energy dissipation:

$$\gamma_s = 3 \rho_s \alpha_s^2 g_0 (1 - e_p^2) \theta_s \left( \frac{4}{d_p} \sqrt{\frac{\theta_s}{\pi}} - \nabla \cdot \mathbf{u}_s \right) \quad (12)$$

$$J_{vis} = -3K_{sg} \theta_s$$

Parameter	Model
Particle pressure	Syamlal $p_s = 2\rho_s\alpha_s^2g_0(1 - e_p)\theta_s$
	Lun $p_s = \rho_s\alpha_s\theta_s + 2\rho_s\alpha_s^2g_0(1 - e_p)\theta_s$
Radial distribution	Sinclair-Jackson $g_0 = \frac{1}{1 - \left(\frac{\alpha_s}{\alpha_{s,max}}\right)^{1/3}}$
	Gidaspow $g_0 = \frac{0.6}{1 - \left(\frac{\alpha_s}{\alpha_{s,max}}\right)^{1/3}}$
	Lun-Savage $g_0 = \left(1 - \frac{\alpha_s}{\alpha_{s,max}}\right)^{-2.5\alpha_{s,max}}$
	Carnahan-Starling $g_0 = \frac{1}{1 - \alpha_s} + \frac{3\alpha_s}{2(1 - \alpha_s)^2} + \frac{\alpha_s^2}{2(1 - \alpha_s)^3}$
Kinetic viscosity	Gidaspow $\mu_{s,kin} = \frac{10\rho_s d_p \sqrt{\theta_s \pi}}{96g_0(1 + e_p)} \left[1 + \frac{4}{5}(1 - e_p)\alpha_s g_0\right]^2$
	Syamlal $\mu_{s,kin} = \frac{\alpha_s \rho_s d_p \sqrt{\theta_s \pi}}{6(3 - e_p)} \left[1 + \frac{2}{5}(1 - e_p)(3e_p - 1)\alpha_s g_0\right]$
	Hrenya-Sinclair $\mu_{s,kin} = \frac{\alpha_s \rho_s d_p \sqrt{\theta_s \pi}}{6(3 - e_p)} \left[1 + \frac{(3e_p - 1)}{2l} + \frac{2}{5}(1 - e_p)(3e_p - 1)\alpha_s g_0 + \frac{5}{4} \frac{1}{(1 - e_p)\alpha_s g_0 l}\right]$
Thermal conductivity	Gidaspow $\kappa_s = \rho_s d_p \sqrt{\theta} \left[ \frac{2\alpha_s^2 g_0 (1 + e_p)}{\sqrt{\pi}} + \frac{9}{16} \sqrt{\pi} \alpha_s^2 g_0 (1 + e_p) + \frac{15}{16} \sqrt{\pi} \alpha_s + \frac{25 \sqrt{\pi} g_0}{64(1 + e_p)} \right]$
	Syamlal $\kappa_s = \rho_s d_p \sqrt{\theta} \left[ \frac{2\alpha_s^2 g_0 (1 + e_p)}{\sqrt{\pi}} + \frac{9 \sqrt{\pi} \alpha_s^2 g_0 (1 + e_p) (2e_p - 1)}{2(49 - 33e_p)} + \frac{15 \sqrt{\pi} \alpha_s}{2(49 - 33e_p)} \right]$
	Hrenya-Sinclair $\kappa_s = \rho_s d_p \sqrt{\theta} \left[ \frac{2\alpha_s^2 g_0 (1 + e_p)}{\sqrt{\pi}} + \frac{9 \sqrt{\pi} \alpha_s^2 g_0 (1 + e_p) (2e_p - 1)}{2(49 - 33e_p)} + \frac{15 \sqrt{\pi} \alpha_s (0.5e_p^2 + 0.25e_p - 0.75 + l)}{(49 - 33e_p)l} + \frac{25}{4(49 - 33e_p)(1 + e_p)l g_0} \right]$

Table 2: Available KTGF models

To calculate the rest of the parameters, a list of the models available on the solver, are summarized in Table 2.

An important remark is that most of the models for the radial distribution introduce strong numerical instabilities due to the singularity when the packing limit is reached. The Carnahan-Starling model (Carnahan and Starling, 1969) is recommended to avoid this issue.

### 3 NUMERICAL METHOD

#### 3.1 The PIMPLE algorithm

The solution algorithm implemented in the present solver is based on a modification of the PISO algorithm (Issa, 1985), called PIMPLE. This procedure improves the convergence and robustness of the first method by introducing under-relaxation factors. This procedure is explained in detail by Passalacqua and Fox (2011).

The operations performed in each time step may be summarized as follows:

1. Store the previous iteration value of pressure, for explicit underrelaxation.
2. Update the  $\partial p / \partial \alpha_s$  field at each cell and face centroids.
3. Solve the  $\alpha_s$  continuity equation and iterate until the pre-defined convergence criterion (or the pre-determined number of iterations) is met.
4. Update the momentum transfer coefficients with the new value of the phase fractions.
5. Solve the  $\theta_s$  granular temperature equation.
6. Compute the phase stress tensors.
7. Solve the phase momentum equations to obtain the predicted values of the velocities at the new time.
8. Start the pressure corrector loop.
9. Repeat the previous steps until the solution satisfies the pre-defined convergence criterion (or the pre-determined number of iterations is reached).

#### 3.2 Numerical Schemes

OpenFOAM® has a wide range of numerical schemes available for the discretization of each term on the conservation equations. This allows the user to select the scheme according to the accuracy needed for a particular problem. For example, for the momentum and phase fraction convective terms ( $\nabla \cdot (\mathbf{u}_i \mathbf{u}_i)$  and  $\nabla \cdot (\alpha_i \mathbf{u}_i)$ ) discretization, we will focus on three numerical schemes. The *limitedLinear* scheme is a limited second order central scheme, with the special version *limitedLinear01* to ensure the bounding between 0 and 1 for the phase fraction convective term and the *limitedLinearV* for vector fields such as the momentum convective term. The fully *upwind* scheme may be the right choice to ensure the stability of the solution, but in most cases, introduces too much diffusivity. Falling between these two methods, a bounded *linearUpwind* method (which is second order accurate) has proven to be robust for most industrial applications.

## 4 RESULTS AND DISCUSSION

### 4.1 Test cases

Two basic test cases were studied to evaluate the performance of drag and KTGF models under different discretization schemes, and then obtain some criteria for the set up of problems with a higher level of complexity.

#### 4.1.1 Column sedimentation

The first test case is a two-dimensional problem which consists of a homogeneous settling gas-solid suspension under the effect of gravity in a vertical column, starting from an uniform solid volume fraction. The simulation was performed with a timestep of  $1.0 \times 10^{-5}$  s on a  $0.05 \times 0.3$  m domain with a grid of  $8 \times 40$  square cells. The initial solid volume fraction is set to 0.3 and the packing limit is specified as 0.63. The numerical scheme adopted for the convective term discretization was full upwind, which was necessary to avoid fluctuations near the packing limit. The continuous phase is air ( $\rho_g = 1.28 \text{ Kg/m}^3$ ,  $\nu_g = 1.328 \times 10^{-5} \text{ m}^2/\text{s}$ ) and the dispersed phase consists of spherical particles with a density of  $\rho_s = 2460 \text{ Kg/m}^3$  and a diameter of  $d_p = 480 \mu\text{m}$ . The results were compared with the ones obtained by [Passalacqua and Fox \(2011\)](#) with the MFIx platform.

Figure 1 shows the solid volume fraction along a vertical centered line at different times. A more diffusive aspect of the solid volume fraction is obtained in the transient stage at  $t = 0.1\text{s}$  due to the upwind numerical scheme in comparison with the MFIx results. Nevertheless, the steady state (reached at  $0.6\text{s}$ ) shows a sharp stratification which is consistent with the expected physical behavior.

Based on the steady state solution, we may conclude that even a scheme with strong numerical diffusion (first order upwind) could be proper to simulate this kind of problems.

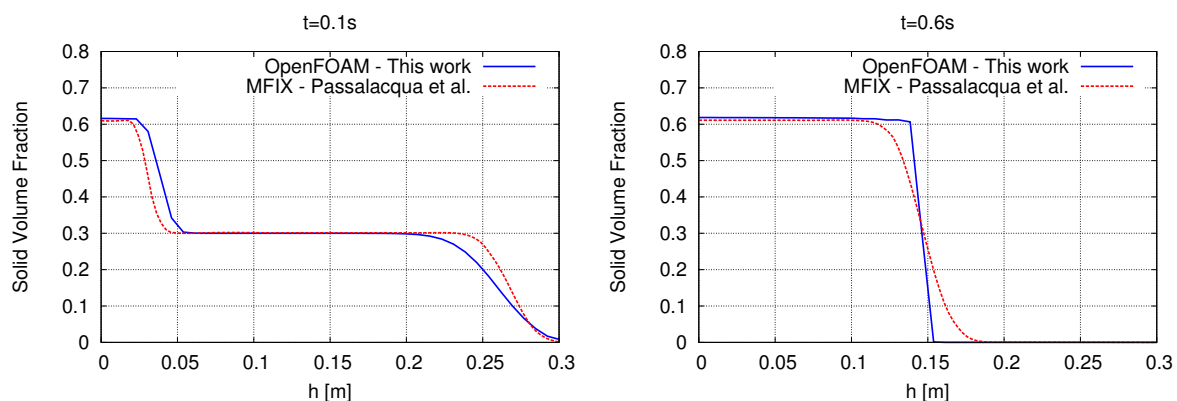


Figure 1: Vertical profile of the solid phase fraction on a transient stage (top) and a steady state (bottom)

#### 4.1.2 Falling block of particles

The second case of study is a falling block of particles in a vertical column that hits the bottom under the effect of gravity. This is a two-dimensional problem for a rectangular domain of 0.05 m wide and 0.2 m high. The grid consists of  $10 \times 40$  structured squares. The continuous phase is air with  $\rho_g = 1.2 \text{ Kg/m}^3$  and  $\nu_g = 1.5 \times 10^{-5} \text{ m}^2/\text{s}$ , while the dispersed phase are solid uniform spherical particles with  $\rho_s = 2000 \text{ Kg/m}^3$  and a diameter of  $d = 400 \text{ }\mu\text{m}$ .

In this problem, the powder modulus was adopted to calculate the elastic stress modulus  $G(\alpha_s)$  in order to obtain the particles pressure as described in Eq. 14 (Bouillard et al., 1989) and slip condition was specified for the solid phase velocity at the walls.

$$\nabla p_s = G(\alpha_s) \nabla \alpha_s \quad (13)$$

$$G(\alpha_s) = \frac{\partial p_s}{\partial \alpha_s} = G_0 e^{[c(\alpha_s - \alpha_{s,max})]} \quad (14)$$

The time evolution of the solid volume fraction are shown in Figure 2. The volume fraction evolves as expected with strong gradients near the packing limit and a flat interface is reached when the solid phase settles completely at  $t = 0.35 \text{ s}$ . Some instabilities on the phase fraction are still present on settled state. This may be due to the mesh size and the numerical scheme adopted (TVD).

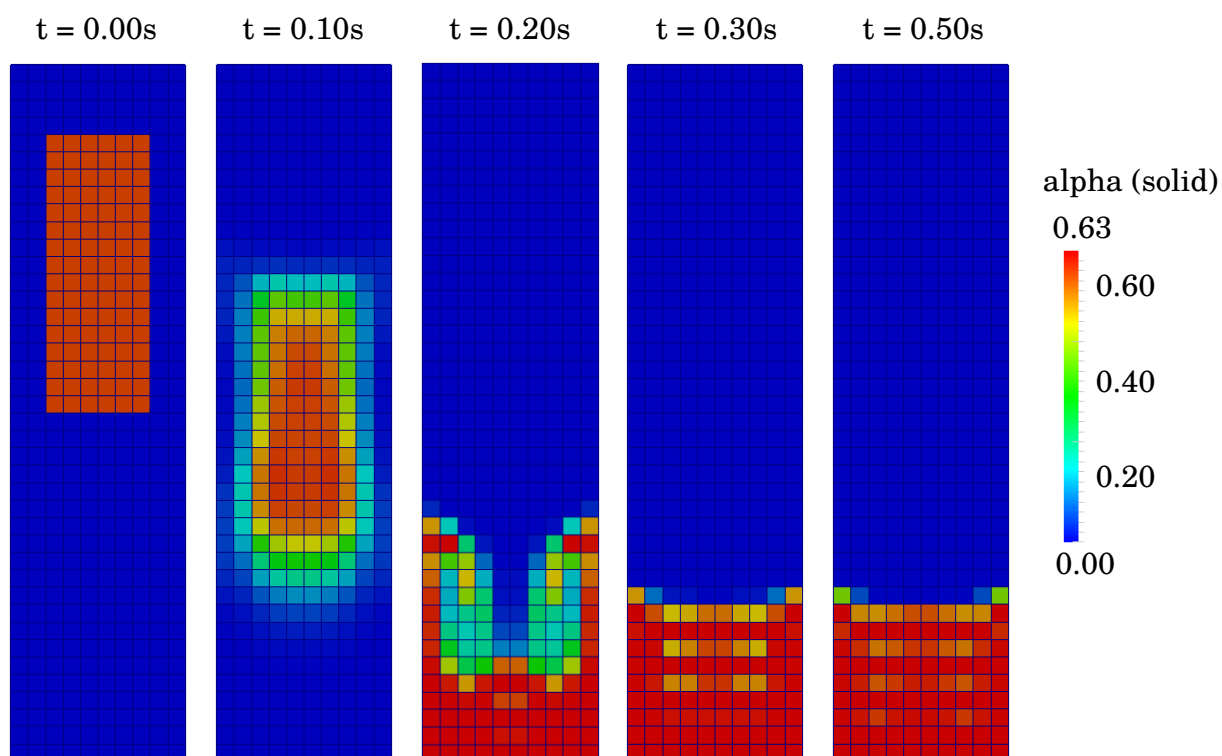


Figure 2: Time evolution of the dispersed phase volume fraction

## 4.2 Fluidized bed

Next, a two-dimensional fluidized bed with Geldart B particles was studied (Figure 3) on a riser configuration. All the model parameters and phase properties are summarized in Table 3.

In this case, we focus our attention in studying the solution with different drag models. Figure 4 shows the mean solid volume fraction in the fluidized region, averaged between  $t = 5s$  and  $t = 30s$  to avoid the start of the fluidization stage. It is clear that most of the solid phase concentrates towards the walls as was expected.

Group	Description	Value
Phase properties	Gas density	1.4 Kg/m <sup>3</sup>
	Gas viscosity	$1.8 \times 10^{-5}$ Pa.s
	Particle density	2000 Kg/m <sup>3</sup>
	Particle diameter	$350 \times 10^{-6}$ m
Geometry	Width	0.138 m
	Height	1 m
	Bed initial height	0.2 m
Numerical method	Grid	14 × 100 (structured squares)
	Timestep	$1.0 \times 10^{-4}$ s
	Overall simulation time	30.0 s
	Time discretization	Second order, implicit
	Momentum discretization	TVD limited linear
	Momentum residual	$1.0 \times 10^{-3}$
	Volume fraction discretization	TVD limited linear
Volume fraction residual	$1.0 \times 10^{-6}$	
KTGF model	Particle pressure	Lun
	Radial distribution	Carnahan-Starling
	Kinetic viscosity	Gidaspow
	Thermal conductivity	Gidaspow
	Restitution coefficient	0.9
Initial and boundary conditions	Vertical inlet gas velocity	0.54 m/s
	Wall solid velocity	slip
	Intel solid volume fraction	0.0
	Outlet pressure	0 Pa
	Initial bed packing	0.58

Table 3: General parameters

Figure 5 shows the radial distribution of solid volume fraction compared with the one obtained by Passalacqua and Fox (2011). All the different drag models show good agreement with slight differences on the minimum solid fraction near the walls, which may be attributed to different boundary conditions for the solid phase velocity.

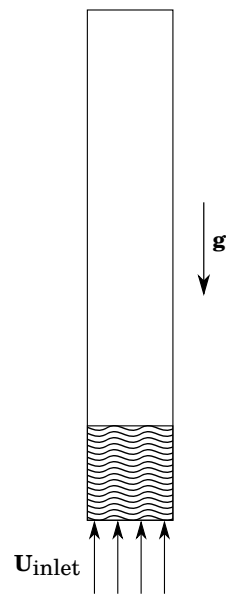


Figure 3: Schematic representation of a fluidized bed problem

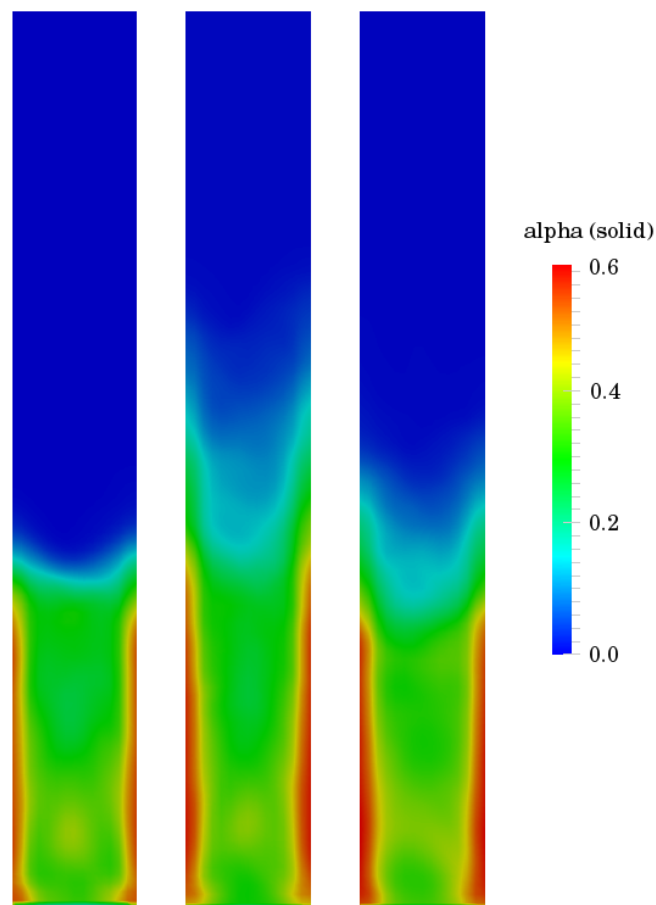


Figure 4: Time-averaged solid volume fraction for different drag models: Syamlal-O'Brien (left), Gidaspow (center), Wen-Yu (right)

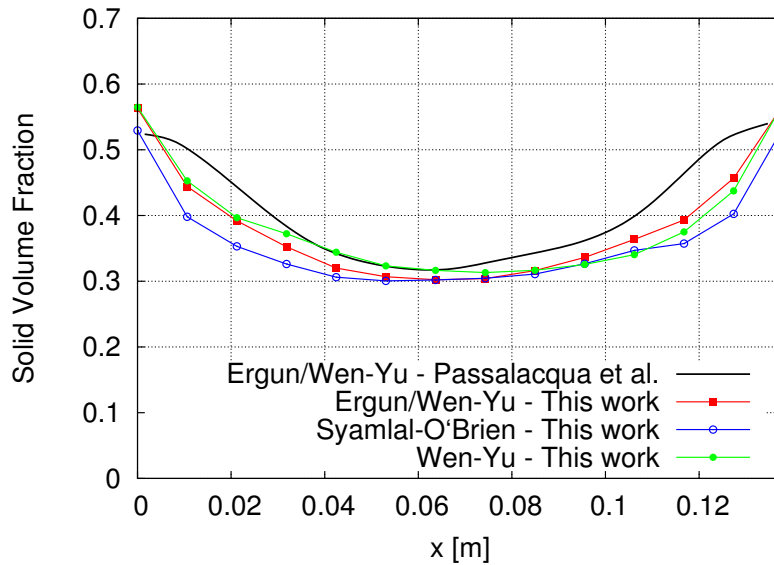


Figure 5: Time-averaged solid volume fraction profile on a horizontal plane at  $y = 0.16$

The results of time-averaged bed height predicted in this work shows a strong dependence on the drag model (see Figure 6). The Syamlal-O'Brien model shows a typical profile for fluidized beds while the Wen-Yu and Gidaspow seems to overestimate the overall effect of the drag force (Ramajo et al., 2010). Figure 7 shows the pressure profile along the height of the riser. The smoothness of this result indicates that the numerical method is stable even near the packing limit. Once again, the Syamlal-O'Brien model predicts a pressure drop of 2500 Pa, which is in agreement with the reported results.

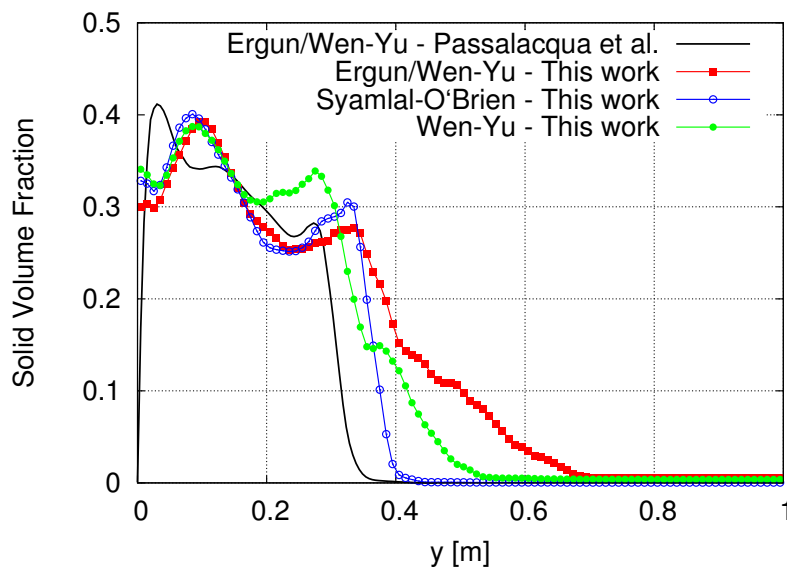


Figure 6: Time-averaged solid volume fraction profile on a vertical centered plane

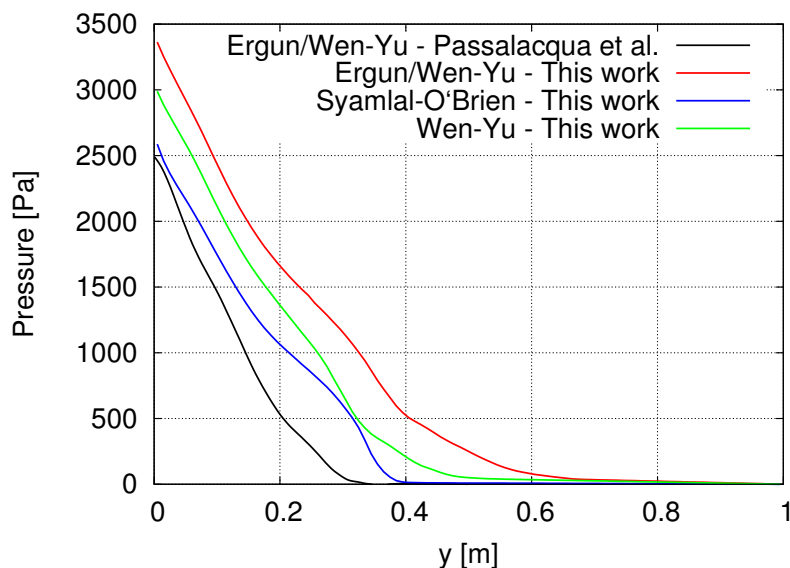


Figure 7: Pressure drop along the vertical length

## 5 CONCLUSIONS

A computational program based on the OpenFOAM<sup>®</sup> platform, was used to solve the Euler-Euler multiphase flow model with kinetic theory closure on two-dimensional laminar standard problems. The implementation on a column sedimentation showed a stable behavior near the packing limit for both transient and steady state, in which a sharp phase segregation profile was obtained. Also, the simulation of a two-dimensional fluidized bed riser showed some level of agreement with published results. We believe that most of the differences could be due to different boundary conditions for the dispersed phase at the walls and the use of a coarse grid. A stable solution was achieved with a TVD momentum discretization scheme and a relatively large time step ( $1 \times 10^{-4}$  s) which indicates that the solver may be a proper tool for industrial scale problems. Finally, a study of different drag models was performed, in which the solutions of the Syamlal-O'Brien model turned out to be similar to the reported data, while Gidaspow and Wen-Yu models seemed to overestimate the drag effect on the fluidized bed height.

**NOTATION**

$c$	compaction modulus
$C_d$	drag coefficient
$C_e$	Syamlal-O'Brien drag coefficient
$d_p$	particle diameter, m
$e_p$	particle restitution coefficient
$\mathbf{g}$	gravity acceleration, m/s <sup>2</sup>
$g_0$	radial distribution coefficient
$G$	elastic stress modulus, N/m <sup>2</sup>
$G_0$	packing elastic stress modulus, N/m <sup>2</sup>
$\mathbf{I}$	identity tensor
$\mathbf{I}_{2D}$	second invariant of the deviatoric stress tensor
$J_{vis}$	transfer rate of energy, Kg/m.s <sup>3</sup>
$K_{ij}$	momentum exchange coefficient, Kg/m <sup>3</sup> .s
$l$	length scale, m
$p$	pressure, Pa
$p_s$	granular pressure, Pa
$Re_p$	relative Reynolds number
$\mathbf{u}_i$	velocity, m/s
$t$	time, s
$v_{rs}$	terminal velocity, m/s

*Greek letters*

$\alpha_i$	volume fraction
$\gamma_i$	energy dissipation, Kg/m.s <sup>3</sup>
$\theta_i$	granular temperature, m <sup>2</sup> /s <sup>2</sup>
$\kappa_i$	diffusion coefficient of granular energy, Kg/m.s
$\lambda_i$	bulk viscosity, Kg/m.s
$\mu_i$	shear viscosity, Kg/m.s
$\mu_{i,col}$	collisional viscosity, Kg/m.s
$\mu_{i,kin}$	kinetic viscosity, Kg/m.s
$\mu_{i,fric}$	frictional viscosity, Kg/m.s
$\nu_i$	kinematic viscosity, m <sup>2</sup> /s
$\rho_i$	density, Kg/m <sup>3</sup>
$\boldsymbol{\tau}_i$	stress tensor, N/m <sup>2</sup>
$\phi$	angle of internal friction

*Subscripts*

$i, j$	general index
$g$	gas
$s$	solid
$p$	particle

## Acknowledgment

Authors want to say thanks to CONICET and UNL (grant CAI+D PI 501-201101-00435 PACT 83)

## REFERENCES

- Almutter A. and Taghipour F. Computational fluid dynamics of a circulating fluidized bed under various fluidization conditions. *Chemical Engineering Science*, 63:1696–1709, 2008.
- Bouillard J., Lyczkowski R., and Gidaspow D. Porosity distributions in a fluidized bed with immersed obstacle. *AIChE J.*, 35:908–922, 1989.
- Carnahan N. and Starling K. Equation of state for nonattracting rigid spheres. *Journal of Chemical Physics*, 51:635–636, 1969.
- Gidaspow D. *Multiphase flow and fluidization: continuum and kinetic theory descriptions*. Academic Press, 1994.
- Issa R. Solution of the implicitly discretized fluid flow equations by operator-splitting. *Journal of Computational Physics*, 62:40–65, 1985.
- Li T., Garg R., Galvin J., and Pannala S. Open-source MFIX-DEM software for gas-solids flows: Part 2 - validation studies. *Powder Technology*, 220:138–150, 2011.
- Min J., Drake J., Heindel T., and Fox R. Experimental validation of cfd simulations of lab-scale fluidized-bed reactor with and without side-gas injection. *AIChE J.*, 56:1434–1446, 2010.
- OpenCFD-OpenFOAM. *Programmer's guide, 1st Edition*, OpenCFD Ltd., United Kingdom, 2010.
- Passalacqua A. and Fox R. Implementation of an iterative solution procedure for multi-fluid gas-particle flow models on unstructured grids. *Powder Technology*, 213:174–187, 2011.
- Ramajo D., Marquez Damian S., Ravicula M., and Nigro N. High density circulating fluidized bed riser: Influence of drag model, kinetic theory and wall slip conditions. *Mecánica Computacional*, 29:3785–3798, 2010.
- Ranade V. *Computational flow modeling for chemical reactor engineering*. Academic Press, 2002.
- Schaeffer D. Instability in the evolution equations describing incompressible granular flow. *Journal of Differential Equations*, 66:19–50, 1987.
- Van Wachem B. *Derivation, implementation, and validation of computer simulation models for gas-solid fluidized beds*. PhD Thesis, Delft University of Technology, 2000.